Cold start characteristics and freezing mechanism dependence on start-up temperature in a polymer electrolyte membrane fuel cell

Yutaka TABE*, Masataka SAITO, Kaoru FUKUI and Takemi CHIKAHISA
Division of Energy and Environmental Systems, Graduate School of Engineering, Hokkaido University
N13 W8, Kita-ku, Sapporo 060-8628, Japan

* Corresponding author. Tel.: +81 11 706 6381; fax: +81 11 706 7889.
E-mail address: tabe@eng.hokudai.ac.jp; N13 W8, Kita-ku, Sapporo 060-8628, Japan.

Abstract

Cold start characteristics of a polymer electrolyte membrane fuel cell are investigated experimentally, and microscopic observations are conducted to clarify the freezing mechanism in the cell. The results show that the freezing mechanism can be classified into two types: freezing in the cathode catalyst layer at very low temperature like −20 ℃, and freezing due to supercooled water at the interface between the catalyst layer and the gas diffusion layer near 0 ℃ like −10 ℃. The amount of water produced during the cold start is related to the initial wetness condition of the polymer electrolyte membrane, because water absorption by the membrane due to back diffusion plays an important role to prevent the water from freezing. It is also shown that after the shutdown of the cold start the cell performance of a subsequent operation at 30 ℃ is temporarily deteriorated after the freezing at −10 ℃, but not after the freezing at −20 ℃. The ice formed at the interface between the catalyst layer and the gas diffusion layer is estimated to cause the temporary deterioration, and the function of a micro porous layer coating the gas diffusion layer for the ice formation is also discussed.

Highlights

- Two freezing types at cold start in and on the surface of a cathode catalyst layer
- Direct observation of the ice formed on the catalyst layer surface
- Temporary performance deterioration at 30 ℃ caused by ice on the surface

Keywords: PEM fuel cell, Cold start, Freezing, Ice, Direct observation, Performance deterioration

1. Introduction

The polymer electrolyte membrane fuel cell (PEFC) is considered a potential candidate for automotive power sources and portable electricity generators because of its characteristics of high efficiency, high power density, low operating temperature, and other advantageous characteristics. Characteristically, PEFCs are also less affected by deterioration at subzero temperature operation than secondary batteries, but low-temperature startability issues of PEFCs remain as an obstacle in need of solution for use of PEFCs in cold regions. Freezing of water produced by the cathode reaction may induce a shutdown at cold start in below zero

temperatures, and it has been reported that this freezing causes various kinds of degradation of the cell performance [1−3].

The research group of the authors have investigated the performance of a PEFC at temperatures below the freezing point by both experiments and simulation, and the initial temperature at which self-starting is possible, which is determined by the balance of the produced heat and water generated due to the reaction, was identified [4]. Cyclic voltammetry studies on the degradation of the electrochemically active Pt area of the cathode catalyst layer due to the ice formation were conducted for a cell containing a membrane with high water content after freezing/thawing cycling [1,2] and during and post-subzero start-up of a PEFC [3]. Here, together with the permanent degradation caused by structural alterations of the cathode catalyst layer [1–3], a temporary deterioration of the cell performance was reported after start-up from subzero temperatures and the warm-up to 25 ℃ with all ice in the catalyst layer melted [3]. Tajiri et al. proposed a strict gas purge process before cold start operation, and estimated the ice distribution in the cathode catalyst layer at the end of cold starting at –30 ℃ at low and high current densities [5]. Recently, cryo-SEM observations were conducted to elucidate further details of the ice distribution in the catalyst layer at –25 ℃ or –20 ℃; these observations were carried out with the examined components kept at very low temperature and in vacuum conditions to avoid thawing and covering by frost deposits [6–9]. At temperatures closer to zero, like –10 ℃, it was reported that the produced water is present in a supercooled state, and that the freezing behavior in a PEFC can be visualized by infrared thermography and it was possible to capture the 2-dimensional propagation in the high temperature region caused by the release of heat due to freezing [10–12]. Thus, the characteristics of the cold start using specific cells and start-up temperatures, and the effects of the water freezing in the cell on the performance deterioration have been reported. Further research, however, is necessary to clarify the effects of the start-up temperature on the cold start characteristics with the operating conditions strictly controlled by gas purging before the cold start, because the characteristics of the operation here are strongly affected by the initial residual water inside the cell [13]. Additionally, the freezing site, the freezing mechanism, and the effect of the start-up temperature on the conditions in the cell have not been fully elucidated, and an understanding of more details of the freezing mechanism would be extremely useful to be able to design the structure of PEFCs and specify the operating conditions that are optimal for cold starting.

This study investigated the effects on the cold start characteristics of a PEFC, of the start-up temperature, current density, and initial residual water in the cell, experimentally. Investigation of the freezing mechanism and its dependence on the start-up temperature was also conducted by direct observations of the inside of the cell, here the cell was disassembled after the cold start shutdown and the distribution of the ice formed in the cell was identified using optical microscopy. Further, the effect of the start-up temperature on the temporary performance deterioration at subsequent non-freezing temperature operation after the occurrence of cold start shutdowns was clarified, and the causes of the deterioration are discussed based on the results of the direct observations.

2. Experimental apparatus and methods

An outline of the single cell with an active area of 25 cm^2 (5 cm × 5 cm) used in this study is shown in Fig. 1, together with a photo of the arrangements inside the thermostatic chamber which will be described further later. A catalyst-coated membrane (CCM) with a 30 μm thick polymer electrolyte membrane and two 10 μm thick catalyst layers was sandwiched between the gas diffusion layers (GDLs), separators with gas flow channels, electricity collectors, and the end-plates of the cathode and anode sides. Here, 0.3 mm thick carbon paper with a micro porous layer on the CCM side was used for the GDLs, and straight channel carbon separators were placed on both sides of the GDLs. The widths of the channels and lands were 1.0 mm, and the channel height was 0.5 mm. The thicknesses of the copper electricity collector overlaid with gold and the stainless-steel end-plates were 3.0 mm and 15.0 mm, so the heat capacity per reaction area of the cell is much larger than that of an ordinary PEFC stack. Thus, the cell temperature controlled by the ambient temperature can be kept fairly constant (isothermal) during the cold start operation in low output conditions. Rubber heaters for rising temperature on the both end-plates and thermocouples for measuring the cell temperature on both separator surfaces at the electricity collector sides were installed.

Fig. 2 shows a schematic view of the apparatus for evaluating the fuel cell performance in this study. The flow rates of the supplied gases: hydrogen, nitrogen, air, and oxygen, were controlled by mass flow controllers installed at each supply line; the pressure of the supplied gases was 0.2 MPa and the exhaust valves were open to the atmosphere. The gas supply lines can be switched to become wet lines by passing a bubbler or to be dry lines, controlled by a three-way valve, and it is also possible to flow the gases bypassing the cell by bypass lines. These basic gas supply lines were used to ensure strict control of the initial residual water conditions in the cell. In the cold start operation below freezing, purpose-installed dry lines which are independent of the basic gas supply lines (not shown in Fig. 2) were used to eliminate uncertainties that could arise from residual moisture in the gas lines. The cell was set vertically in a thermostatic chamber (HITACHI, EC-25MTP) with a controllable temperature range of –30 to 100 ℃ with ± 0.3 ℃ accuracy, and the temperatures of the cell and the supply gas were controlled by the chamber temperature. An optical microscope for high or low magnification (HIROX, SH-4500 or LEICA, Z16APO) was installed in the chamber to enable direct observations of the cell components, and a LED light source with low heating value was used as the light source for high magnification observations to prevent even small ice crystals from melting due to thermal effects of the light. The focus and the observation positions were adjusted using a motorized XYZ stage movable in the low-temperature environment, and this was also installed in the thermostatic chamber. The thermostatic chamber has a window and two handling holes at the front, which make it possible to disassemble the cell and observe the component surfaces inside the cell (without removal from the cell) using the optical microscope and at the below freezing temperatures. The cell resistance was measured by an alternating impedance meter at 1 kHz, and the cell voltage, cell resistance, as well as the temperatures of the cell and the supply gas were recorded on a computer.

The procedures of the experiment are outlined in Fig. 3. Because the initial residual water strongly affects the cold start characteristics [13], the initial conditions of the water in the cell before the cold start were carefully controlled by the procedure described next. After an aging process to enhance the performance of an unused CCM, a dry purge, lasting about 5 minutes,

with dry nitrogen was conducted to remove the liquid water in the cell, followed by a wet purge with humidified nitrogen to achieve an equilibrium state of the CCM until the resistance was maintained at a steady level for 3 to 5 hours. Four humidification conditions of the nitrogen were used: a bubbler temperature of 30 ℃ and cell temperatures of 60 ℃ (relative humidity of nitrogen 22 %), 50 ℃ (RH 35 %) or 35 ℃ (RH 76 %), and a bubbler temperature of 32 ℃ cell temperature 60 ℃ (RH 24 %). After the wet purge and cooling the cell and the chamber temperatures to the temperature of the experiment, –20 ℃ or –10 ℃, cell operation was initiated and continued at a constant current density until the operation shut down, the point where the cell voltage dropped away completely. The anode and the cathode supply gases were dry hydrogen and dry air, with flow rates of 140 and 330 standard cc min^{-1} (SCCM) respectively. Then, for direct observations of the inside of the cell, the cell was disassembled and the component surfaces were observed by the optical microscope installed in the thermostatic chamber. In the investigation of the subsequent cell performance at ordinary temperatures, the cell was heated to 30 ℃ with an about 2 ℃ min^{-1} rate of temperature increase, and the cell performance at a constant current density was measured. The anode and the cathode supply gases at the normal temperature operation were humidified hydrogen and air with relative humidity 100 %, and flow rates of 500 and 2000 SCCM respectively.

3. Results and discussion

3.1. Cold start characteristics and the effect of start-up temperature

Measured cold start characteristics, the cell voltage and the cell resistance changes, at –20 °C and –10 °C are shown in Fig. 4. Humidified nitrogen with relative humidity 22 % was used in the wet purge (details above) here at 60 °C, and the applied current density was initially increased for 80 seconds followed by a constant value of 0.04 A cm^{-2}. After the start of operation, the cell resistance decreases, and after a minimum around 80 seconds the cell voltages increase gradually. This is because the water produced by the cathode reaction humidifies the polymer electrolyte membrane due to back diffusion; the membrane resistance comprising a large part of the cell resistance becomes smaller with wetter states [14]. The difference in the initial cell resistance at 0 seconds, between –20 ℃ and –10 ℃, is caused by the temperature dependent behavior where the membrane resistance increases with decreasing temperature at the same wet state [14]. The cell resistance at –20 ℃ approaches a steady value around 250 seconds after the start of the operation, and then increases slightly before the cell voltage rapidly falls off and operation stops. The slight increase in the cell resistance around 250 seconds makes a small contribution to the drastic voltage drop, and this shutdown of the cold start can be considered to be caused by the freezing of the water produced in the cell, here the formed ice induces a decrease in the effective reaction area or an interruption in the reaction gas supply. The cell resistance and the voltage at –10 ℃ are nearly constant from 300 to 400 seconds, and the operation shuts down around 580 seconds. This can be explained with previous research by the authors showing that the water produced by the cathode reaction is at a supercooled liquid state in the cell at –10 ℃ relatively-near to zero [10]. Thus, the cold start

characteristics at –20 °C and –10 °C are governed by different phenomena, and a longer operation at –10 °C is possible before the shutdown with a same initial wet condition.

Experiments with operation at three relative humidities of the nitrogen in the wet purge process, 22, 35 and 76 %, were conducted, and the relationships between the cell resistances just before the cold start operation at the three wet conditions of the polymer membrane and the operation periods (expressed by the amount of water produced) were investigated. The experimental results of the 0.04 A cm^{-2} cold start at –20 °C and –10 °C are plotted in Fig. 5. The period of operation is here converted to the estimated amount of water produced by the cathode reaction. These amounts were calculated from the period of operation and the current density, and the amounts during the total operation and during the membrane rehydration (this could also be termed "water uptake by the membrane" or "water back diffusion into the membrane") were plotted. The period of the membrane rehydration was defined as the period when the cell resistance was decreasing. The abscissa is the cell resistance just before the cold start; the leftmost two data points for each condition (two of each of the open and solid triangles and circles) are by the RH 76 % purge, the following two by the RH 35 %, and the remaining (rightmost data points) by the RH 22 % purges. The estimated amounts of the produced water during the membrane rehydration (shown as solid plots (dots and triangles) and broken lines in Fig. 5) become larger as the cell resistances before the cold start increase, both at –20 °C and –10 °C, and they appear to be clearly correlated. This is because the dryer membrane with the higher initial cell resistance has a larger capacity to absorb the water produced by the reaction. Comparing the water amounts produced during the membrane rehydration at –20 °C and –10 °C, the amounts at –10 °C are larger with the same cell resistance before the cold start. One factor contributing this difference is the temperature dependence of the membrane resistance as mentioned above: the initial cell resistance at –10 °C is about 1 Ω cm^2 lower than that at –20 °C with the same wet condition in Fig. 5. Even allowing for this temperature dependence, the amounts of the water at –10 °C are still larger, and this suggests that the freezing at –20 °C occurs before the produced water uptake by the membrane is completely finished. The estimated amount of produced water during the complete operation at –20 °C (open circles in Fig. 5) also increases to about 1.4 mg cm^{-2} with an increase in the initial cell resistance, while that at –10 °C (open triangle in Fig. 5) reaches 2.0 mg cm^{-2} but with some variation.

To examine the characteristics from the end of the membrane rehydration to the shutdown, Fig. 6 shows the estimated amounts of produced water following the end of the membrane rehydration in the experiments as in Fig. 5. The amounts after the membrane rehydration at –20 °C are very similar for the various cell resistances before the cold start operation, but there is great variability among the amounts of the –10 °C operation. These results indicate that after the end of the membrane rehydration the produced water that is not absorbed on the membrane immediately freezes at –20 °C while the water may remain as supercooled water at –10 °C, and this then causes the larger amounts of produced water and the larger variations at –10 °C in Fig. 6.

3.2. Observation of ice distribution and evaluation of the freezing mechanism

The cold start characteristics of PEFCs depend on the start-up cell temperature as shown in Fig. 4, and the differences, especially after the membrane rehydration, are mainly caused by the different freezing mechanisms at –20 °C and –10 °C. Before attempting a more detailed discussion of the freezing mechanism using the direct observation of the ice formed inside the cell, experiments were performed controlling the amount of residual water in the cell after the shutdown at the cold start by the start-up current density. This was done because the expected differences in the ice distribution at –20 °C and –10 °C may be affected not only by the freezing mechanism but also by the amount of the residual water, e.g. the longer operation during the cold start at –10 °C compared with that at –20 °C in Fig. 4 may be a cause of the larger amount of the ice observed in the cell.

The cell voltage and the cell resistance changes for various current densities at –20 °C and –10 °C are shown in Fig. 7. Humidified nitrogen with relative humidity 24 % was used in the wet purge. Table 1 lists the amounts of residual water estimated to be generated during the total operation and from the end of the membrane rehydration till the shutdown. The amount of residual water was estimated as the produced water minus the water removed by the reactant gases, here it was assumed that a portion of the produced water during the cold start is removed by the saturated reactant gases exiting the cell [15]. In this study, only the amount of water removed by the dry cathode gas was considered. The amounts remaining after operation at the various current densities in Table 1 show no clear correlation of the current density with the estimated amount of residual water during the total operation but there is a correlation with that generated after termination of the membrane rehydration till the shutdown both at –20 °C and –10 °C. The higher operating current densities decrease the estimated amount of residual water after the membrane rehydration. It can be assumed that all of the residual water is absorbed by the membrane during the beginning membrane rehydration period, whereas the residual water is released and freezes mainly in the cathode components outside the membrane after the end of the membrane water uptake, and this ice disrupts the cell operation. The results suggested that at the higher current densities the effect of the ice formed at the cathode side on an increase in the concentration overpotential becomes larger and the capacity of the cathode components to maintain the ice without a shutdown decreases. The larger amounts of residual water after the membrane rehydration at –10 °C is considered to be caused by a process where the produced water is maintained in a supercooled state for some time before the freezing.

After the shutdown of the cold start, the cell was disassembled and the surfaces of the cell components were subjected to detailed observations by the optical microscope at the sub-zero temperature of the thermostatic chamber. Figs. 8(a) and (b) are examples of micrographs of the cathode catalyst layer surface at –20 °C and –10 °C. The start-up current densities were 0.02 A cm^{-2} at –20 °C and 0.12 A cm^{-2} at –10 °C with the similar estimated amounts of the residual water in the cathode components after the membrane rehydration in Table 1. Much ice was observed across the catalyst layer surface after the shutdown at –10 °C as shown in Fig. 8(b); however, only few ice crystals were observed at –20 °C. The micrograph in Fig. 8(a) is a rare example with small ice crystals at –20 °C, generally no ice was observed here. In the observations of this study, no ice was seen on the surface of the other components such as in the micro porous layer (MPL) or in the gas diffusion layer (GDL). Ice distributions similar to those in Fig. 8 were also confirmed under the other current density conditions. Overall, it

may be concluded that the differences in the ice distribution described above would be caused by the start-up temperature of the cold start and not by the amount of residual water.

Fig. 9 is a schematic representation of the cross-sectional ice distribution and the freezing mechanism suggested by the experimental results. The produced water during the cold start at –20 °C freezes only inside the cathode catalyst layer, Fig. 9(a), and this causes the shutdown of the cell operation. The produced water at the –10 °C cold start reaches the interface between the catalyst layer and the MPL where it remains as a supercooled liquid water film for some time before it freezes, (Fig. 9(b)), this is a reason why the released heat of solidification due to the freezing can be detected by infrared thermography [10–12]. The freezing at the interface triggers the operation shutdown, and in total the freezing mechanism and cold start characteristics differ, depending on whether supercooled water can exist in a cell. The water produced by the cathode reaction passes through the cathode catalyst layer and freezes from the surpercooled state at the interface between the catalyst layer and the MPL at temperatures near zero like at –10 °C, while at lower temperatures, like at –20 °C, the produced water freezes immediately near the reaction sites inside the cathode catalyst layer. Some experimental results of cell characteristics affected by the cell structure near the catalyst layer were obtained at –10 °C, and these support the suggestion that the produced water freezes outside the cathode catalyst layer at –10 °C; put differently, a weaker clamping pressure of the cell increased the operation period of the –10 °C cold start and there was an abrupt increase in the cell resistance measured at the shutdown due to this freezing (not appears in Fig. 4). This behavior can be explained as the space allowing the supercooled water to exist at the interface between the catalyst layer and the MPL becomes larger with a weaker contact pressure and the freezing of a larger amount of liquid water increases the contact resistance between the catalyst layer and the MPL significantly.

3.3. Effect of freezing on the performance of subsequent operation at normal temperature

After the shutdown at the cold start, a deterioration of the cell performance sometimes appears at the subsequent operation at relatively-low temperatures above zero like at 30 °C. This corresponds to a temporary deterioration recoverable by the operation at high temperature, 70 °C, with humidified hydrogen and air with relative humidity 100 % for 2 hours [3] or by the dry nitrogen purge with flow rate of 3000 SCCM for 5 minutes (will be shown later), but the causes of this temporary deterioration after the cold start have yet to be elucidated fully. In this section, the deterioration of the cell performance in subsequent operation at 30 °C was investigated after the occurrence of a shutdown due to cold start at –20 °C and –10 °C, and the causes are discussed.

After the shutdown at the cold start, the cell was heated to 30 °C and operation resumed with the cell temperature kept fairly constant (as outlined in Fig. 3). Fig. 10 shows the results before and after the cold start shutdown with the cold start conditions of the experiments in Fig. 8, where the amounts of residual water in the cathode side after the –20 °C and –10 °C shutdown are estimated to be similar. The applied current density was increased to 0.50 A cm^{-2} during the first 300 seconds of the operation before and after the cold start shutdown. The broken lines are the cell voltages before the cold starting, and the solid lines are those after. The plots clearly show that the cell voltage after the shutdown at the –10 °C cold start

does not recover to the value before the cold start, while there is little difference between the voltages before and after the cold start shutdown at –20 °C. This deterioration after the –10 °C shutdown could be recovered by the dry nitrogen purge with flow rate of 3000 SCCM for 5 minutes, and very similar cell resistances in the range from 0.08 to 0.09 Ω cm^2 were recorded during all of the operations at 30 °C (not shown in Fig. 10). These results indicate that the large amount of liquid water melted from the ice at the interface between the cathode catalyst layer and the MPL at –10 °C limits the gas diffusion in the operation at 30 °C, but that the ice formed in the catalyst layer in the cold start at –20 °C does not affect the gas diffusion after the temperature rises to 30 °C. It was also confirmed that the cell voltages under the other current density conditions behaved similarly to those shown in Fig. 10 and that the temporary deteriorations could be recovered by the dry nitrogen purge.

To investigate the effect of the residual water on the surface of the cathode catalyst layer, the decreases in the cell voltage after the shutdown of the –10 °C cold start were compared between using 0.3 mm thick carbon papers with and without an MPL as the cathode GDL and the results are shown in Fig. 11. The current densities at the cold start and the operation at 30 °C were 0.04 A cm^{-2} and 0.50 A cm^{-2}, respectively. The cell voltages before the cold starts (broken lines) show lower cell voltages of the cell without the MPL. This was a common tendency also observed in other experiments, and corresponds to the generally-recognized effect that there is less flooding with an MPL. The voltage of the cell without the MPL after the cold start shutdown was also lower and operation was soon terminated, as shown by the red solid line in Fig. 11. This supports the above interpretation that the liquid water on the surface of the cathode catalyst layer, which is affected by existence of the MPL, induces the temporary deterioration of the cell performance after the shutdown of the cold start.

Figs. 12(a) and (b) are examples of photos of the cathode catalyst layer surface after the shutdown of the cold start at –10 °C using the GDL with and without the MPL. The start-up conditions are the same as those of the cold start in Fig. 11, and the observations were conducted for a wider area with lower magnification than in Fig. 8 to investigate the ice distribution on the catalyst layer surface. Ice was observed only on the surface of the catalyst layer in both cases (Figs. 12(a) and (b)), but the clear differences in the ice distribution were confirmed. Larger amounts of ice forms under the channels than under the lands after the cold start shutdown of the cell with the MPL (ice is shown as the scattered white regions in Fig. 12(a)), while the ice is distributed all over the catalyst layer surface in the cell without the MPL (ice shown as thinly white layers in Fig. 12(b)). This suggests that the MPL acts to limit the water amount on the surface of the catalyst layer especially under the lands, due to the less free space between the catalyst layer and the MPL with the higher contact pressure. The wider ice distribution of the cell without the MPL is estimated to result from the poorer direct contact and the larger space between the catalyst layer and the GDL because of the rougher surface of the GDL compared with that of the MPL. The larger space at the interface may allow the larger amount of liquid water to accumulate at the interface and act to disturb the oxygen supply to the cathode catalyst layer before and after the cold start shutdown.

Experimentally suggested cross-sectional images are shown in Fig. 13, highlighting the effect of the liquid water at the interface between the catalyst layer and the MPL or the GDL on the oxygen supply in the air during the operation at 30 °C. In the operation using the GDL with the MPL at a normal temperature (Fig. 13(a)), the MPL limits the accumulation of water

on the surface of the catalyst layer and promotes the transport of the produced water to the GDL, and this enables a stable operation with little liquid water near the cathode catalyst layer. The direct contact of the GDL with the catalyst layer without the MPL results in a lager space due to the more irregular GDL surface, and this space allows a larger amount of liquid water to remain on the catalyst layer surface, decreasing the cell performance (Fig. 13(c)). In the cold start operation at a temperature relatively-near to zero like –10 ℃, the produced water would accumulate in a supercooled state in the constricted space due to the low temperature, and after freezing the ice expands beyond the limitations of the space because of the freezing. After heating to a higher temperature (here 30℃), the ice melts and a large amount of liquid water remains on the surface of the cathode catalyst layer, and this blocks the oxygen supply to the catalyst layer, resulting in the temporary deterioration of the cell performance (Figs. 13(b) and (d)). In the case of the operation without the MPL after the cold start shutdown, the larger space on the catalyst layer surface also allows the larger amount of liquid water to spread across and remain on the surface and this liquid water causes the more pronounced deterioration in cell performance after the cold start shutdown (Fig. 13(d)) than in the operation with the MPL (Fig. 13(b)). This discussion allows the conclusion that it is critically important to control the ice formation and the liquid water from melting ice on the surface of the cathode catalyst layer to suppress the temporary deterioration of the cell performance after cold starts.

4. Conclusions

The cold start characteristics of a PEFC were investigated experimentally, and the mechanisms of the freezing in the cell and the temporary deterioration of the cell performance after the cold start shutdown are discussed based on the results of direct observations of the inside of the cell. The major conclusions may be summarized as follows:

1. The cold start characteristics can be classified into two types depending on the start-up temperature. Freezing starts near the end of the membrane rehydration by the produced water at very low temperatures like −20 ℃ and this results in the shutdown here. Near 0 ℃, like at −10 ℃, the produced water after the membrane rehydration remains as supercooled water before it freezes after some holding time and then the shutdown occurs.
2. Few ice crystals at –20 ℃ and a substantial ice layer at –10 ℃ are formed only on the surface of the cathode catalyst layer after the shutdown following the cold starts. This indicates that the produced water freezes only inside the cathode catalyst layer at –20 ℃, but that the water produced at –10 ℃ reaches the interface between the cathode catalyst layer and the micro porous layer (MPL) coating the gas diffusion layer, and then this supercoolded water film freezes.
3. There is no temporary performance deterioration in the subsequent operation at 30 ℃ after the shutdown of the –20 ℃ cold start but the performance after the –10 ℃ shutdown results in a poorer performance. Very similar cell resistances were measured before and after the cold starts, indicating that the oxygen supply to the reaction area after the temperature rises to 30 ℃ is less affected by the ice formed in the catalyst layer in the –20 ℃ cold start, but after the –10 ℃ cold start performance is limited by the liquid water melted from the large amount of the ice at the interface between the cathode catalyst layer and the MPL.

4. The performance of the cell without an MPL before and after the –10 °C cold start is poorer than with the MPL. Ice covers the catalyst layer surface after the cold start shutdown of the cell without the MPL, and less deposits under the lands than under the channels when the cell is equipped with the MPL. These results suggest that the MPL limits the liquid water accumulation on the surface of the catalyst layer due to the better contact between the catalyst layer and the MPL, and this functions to improve the cell performance and suppresses the temporary deterioration after the cold start.

Acknowledgments

This research was partly conducted as a collaborative project with Nissan Motor Co. Ltd. The authors thank the researchers participating in this work for helpful comments on the cold start experiments.

References

[1] E.A. Cho, J.-J. Ko, H.Y. Ha, S.-A. Hong, K.-Y. Lee, T.-W. Lim, I.-H. Oh, J. Electrochem. Soc. 150 (12) (2003) A1667-A1670.
[2] E.A. Cho, J.-J. Ko, H.Y. Ha, S.-A. Hong, K.-Y. Lee, T.-W. Lim, I.-H. Oh, J. Electrochem. Soc. 151 (5) (2004) A661-A665.
[3] S. Ge, C.-Y. Wang, J. Electrochem. Soc. 154 (12) (2007) B1399-B1406.
[4] Y. Hishinuma, T. Chikahisa, F. Kagami, T. Ogawa, JSME Int. J., Series B 47 (2) (2004) 235-241.
[5] K. Tajiri, Y. Tabuchi, C.-Y. Wang, J. Electrochem. Soc. 154 (2) (2007) B147-B152.
[6] J. Li, S. Lee, J. Roberts, Electrochim. Acta 53 (2008) 5391-5396.
[7] E.L. Thompson, J. Jorne, W. Gu, H.A. Gasteiger, J. Electrochem. Soc. 155 (6) (2008) B625-B634.
[8] E.L. Thompson, J. Jorne, W. Gu, H.A. Gasteiger, J. Electrochem. Soc. 155 (9) (2008) B887-B896.
[9] M. Saito, Y. Tabe, T. Chikahisa, ECS Trans. 25 (1) (2009) 773-779.
[10] Y. Tabe, H. Nakamiya, K. Kikuta, T. Chikahisa, F. Kagami, K. Yoshizawa, Proceedings of the 13th International Heat Transfer Conference [1/1 (CD-ROM) SOL-08], 2006, pp. 1-8.
[11] Y. Ishikawa, T. Morita, K. Nakata, K. Yoshida, M. Shiozawa, J. Power Sources 163 (2007) 708-712.
[12] Y. Ishikawa, H. Hamada, M. Uehara, M. Shiozawa, J. Power Sources 179 (2008) 547-552.
[13] K. Tajiri, C.-Y. Wang, Y. Tabuchi, Electrochim. Acta 53 (2008) 6337-6343.
[14] T.E. Springer, T.A. Zawodzinski, S. Gottesfeld, J. Electrochem. Soc. 138 (8) (1991) 2334-2342.
[15] S. Ge, C.-Y. Wang, Electrochem. Solid-State Lett. 9 (11) (2006) A499-A503.

Table 1 Amount of the residual water generated in the total operation and after the membrane rehydration.

Fig. 1. Experimental apparatus and photo of the inside of the thermostatic chamber.

Fig. 2. Schematic outline of the developed arrangement for evaluating the cold start performance and the ice formation inside the cell.

Fig. 3. Experimental procedures of the cold start, the direct observation, and the normal temperature operation.

Fig. 4. Cell voltages and resistances for the 0.04 A cm^{-2} cold start operation at –20 °C and –10 °C.

Fig. 5. Amount of water produced in the total operation and in the membrane rehydration at −20 °C and −10 °C; the abscissa is the cell resistance before the cold start.

Fig. 6. Amount of water produced during the period from the end of the membrane rehydration till the time of the stop of the operation at −20 °C and −10 °C.

Fig. 7. Cell voltages and resistances for the cold start operation of various current densities at –20 °C and –10 °C.

Fig. 8. Micrographs of the cathode catalyst layer surface after the shutdown at −20 °C and −10 °C.

Fig. 9. Experimentally suggested images of the cross-sectional distribution of ice at the shutdown after the cold start at −20 °C and −10 °C.

Fig. 10. Plot of the cell performance at 30 °C before and after the occurrence of shutdown due to the cold start at −20 °C and −10 °C.

Fig. 11. Plot of the cell performance at 30 °C before and after the occurrence of shutdown due to the cold start with and without the MPL.

Fig. 12. Photos of the cathode catalyst layer surface after the shutdown of the cold start at −10°C with and without the MPL.

Fig. 13. Experimentally suggested images of the cross-sectional distribution of liquid water at normal operation and after the cold start shutdown operation.

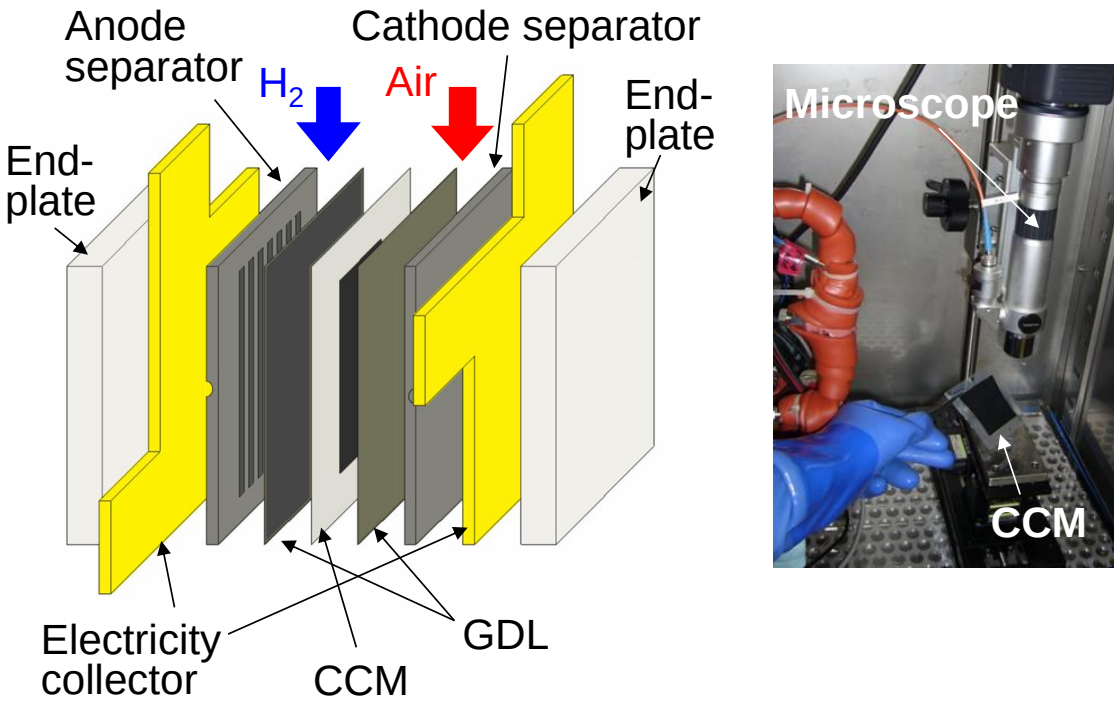

Fig. 1. Experimental apparatus and photo of the inside of the thermostatic chamber.

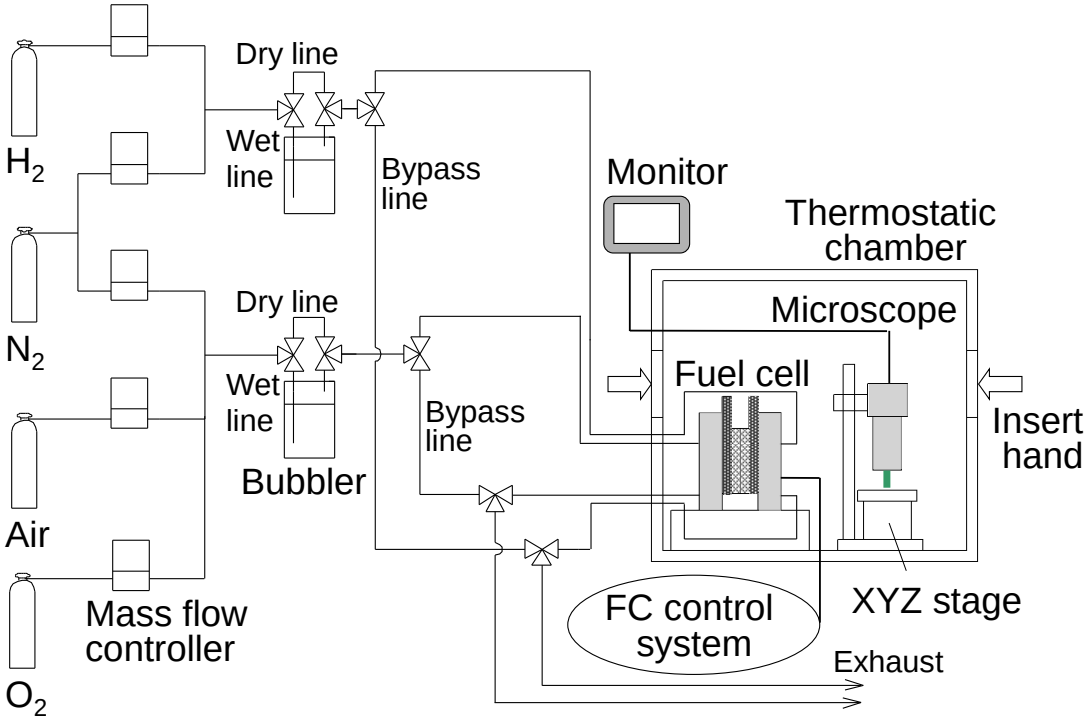

Fig. 2. Schematic outline of the developed arrangement for evaluating the cold start performance and the ice formation inside the cell.

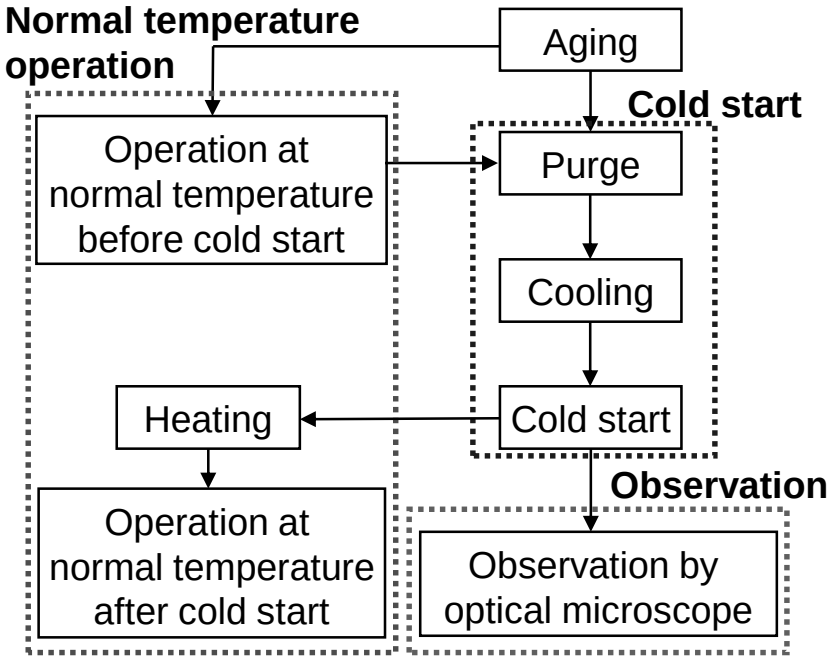

Fig. 3. Experimental procedures of the cold start, the direct observation, and the normal temperature operation.

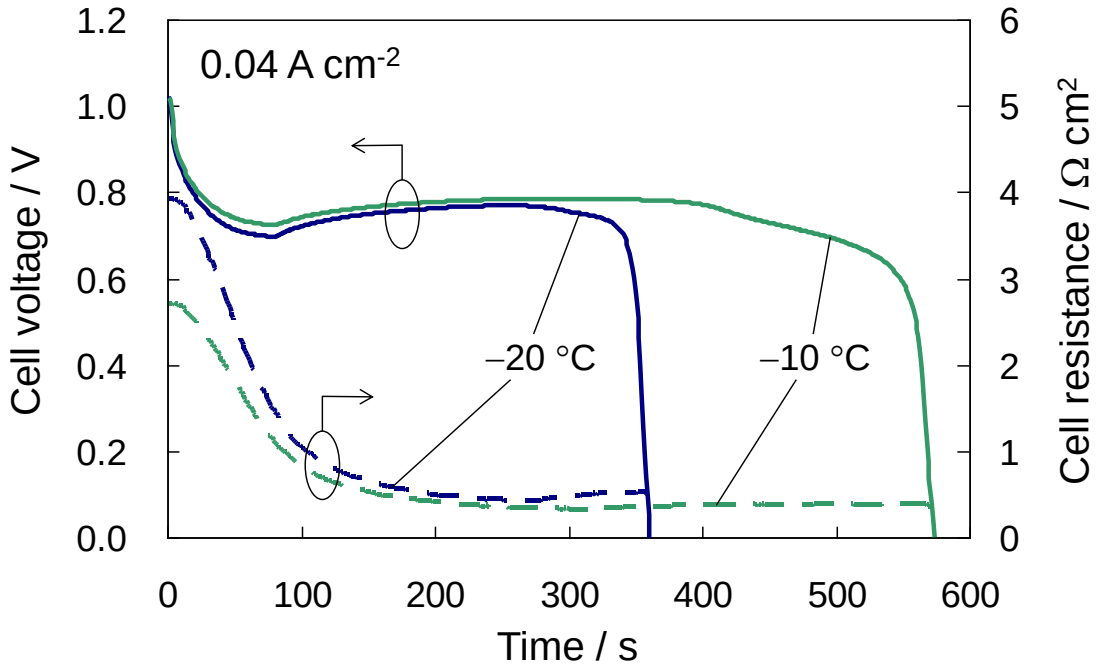

Fig. 4. Cell voltages and resistances for the 0.04 A cm^{-2} cold start operation at –20 °C and –10 °C.

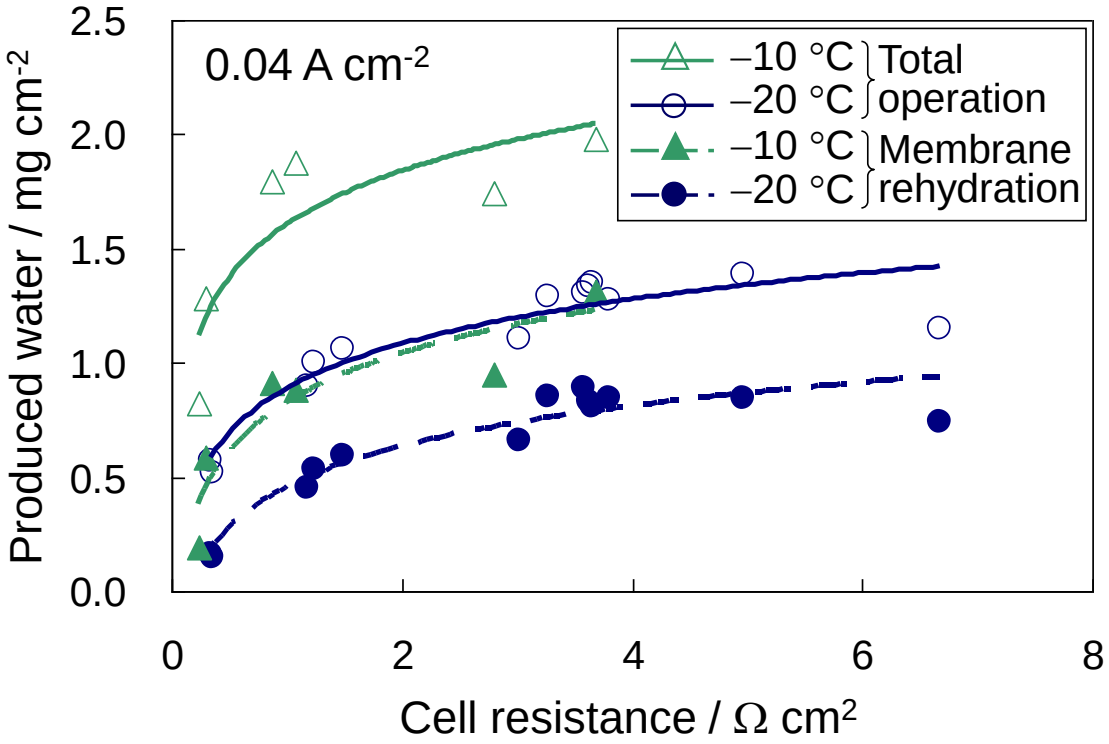

Fig. 5. Amount of water produced in the total operation and in the membrane rehydration at −20 °C and −10 °C; the abscissa is the cell resistance before the cold start.

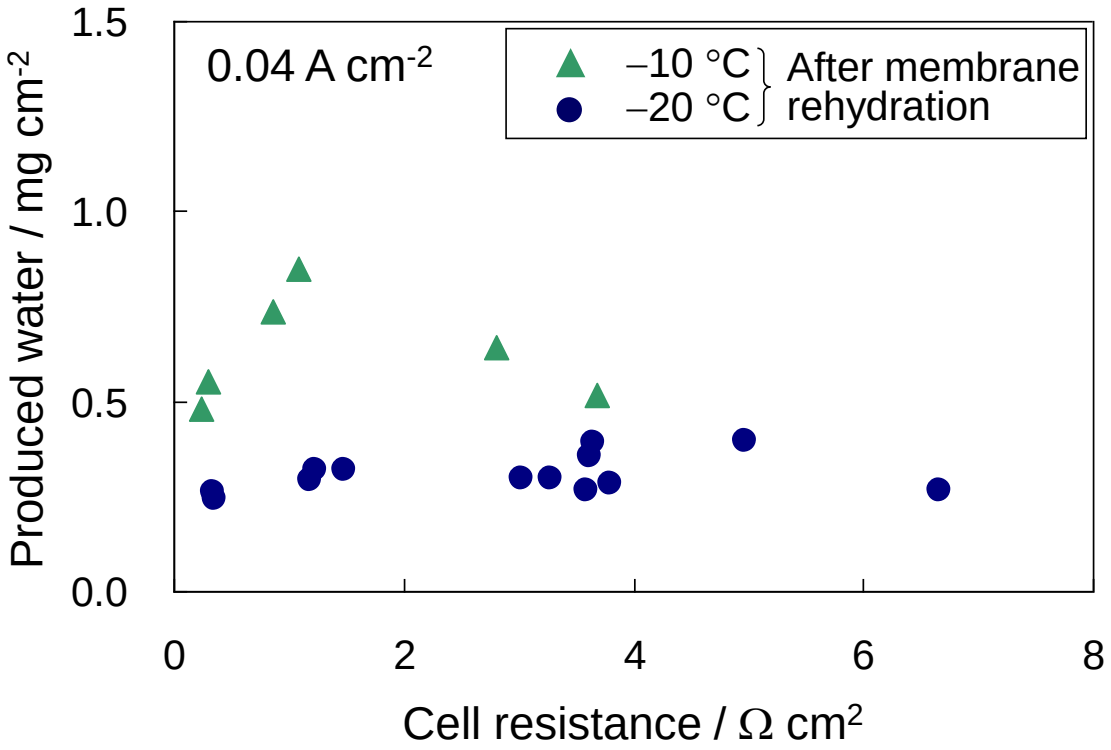

Fig. 6. Amount of water produced during the period from the end of the membrane rehydration till the time of the stop of the operation at −20 °C and −10 °C.

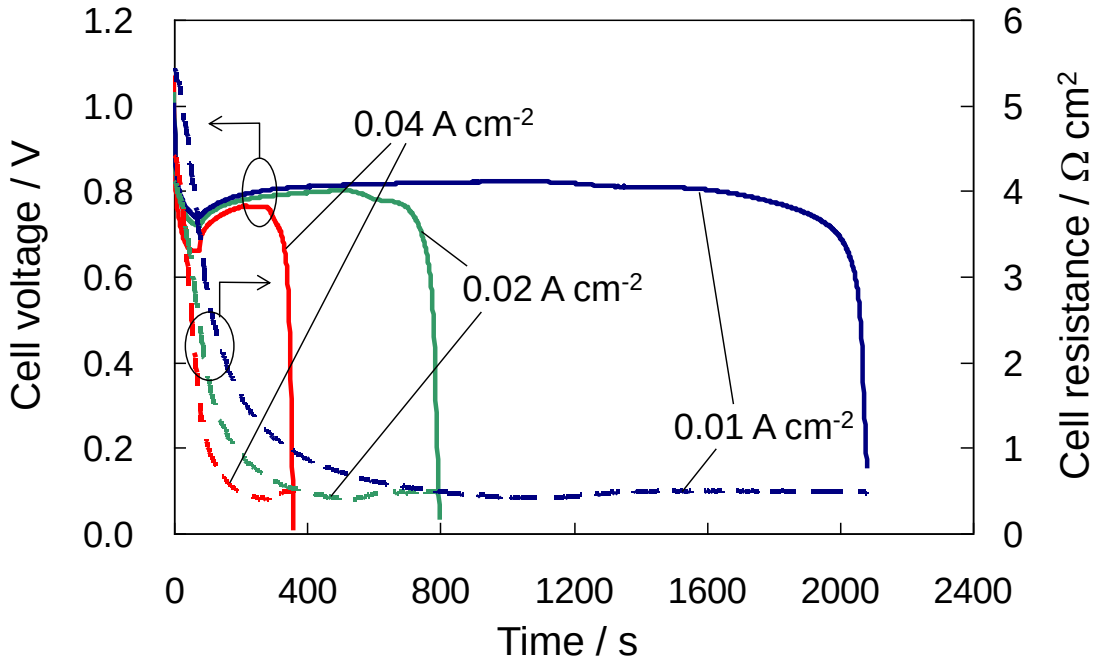

(a) −20 °C

Fig. 7. Cell voltages and resistances for the cold start operation of various current densities at –20 °C and –10 °C.

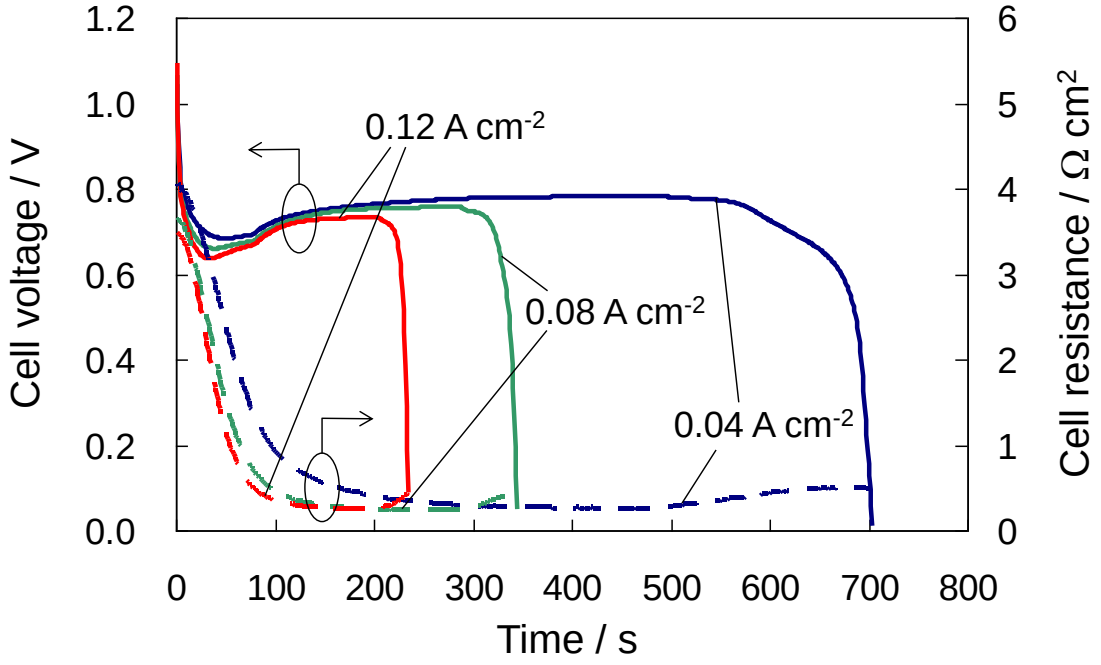

(b) −10 °C

Fig. 7. Cell voltages and resistances for the cold start operation of various current densities at –20 °C and –10 °C.

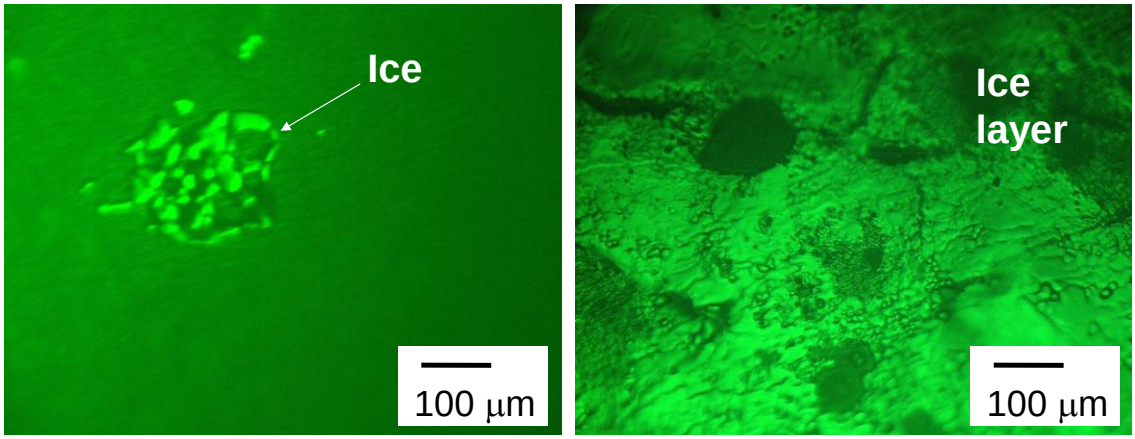

(a) −20 °C (b) −10 °C

Fig. 8. Micrographs of the cathode catalyst layer surface after the shutdown at −20 °C and −10 °C.

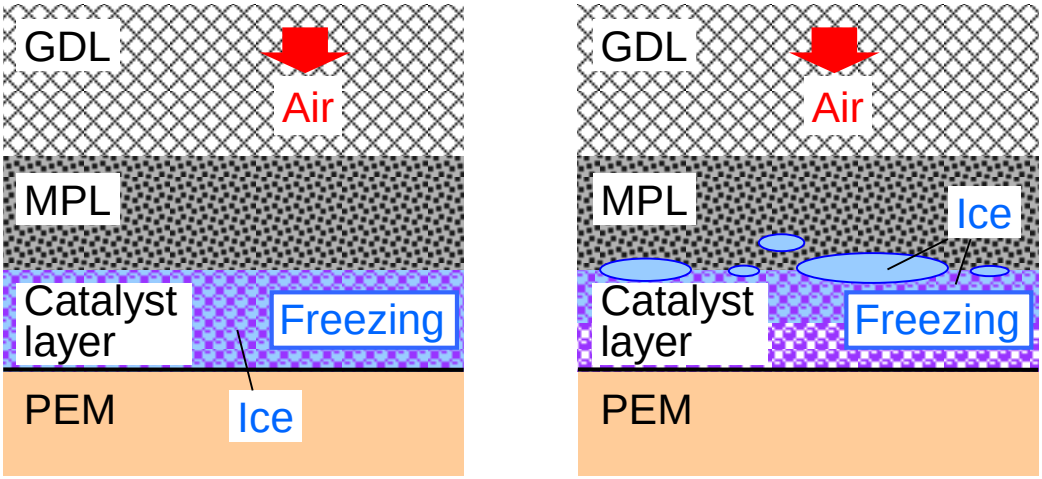

(a) −20 °C (b) −10 °C

Fig. 9. Experimentally suggested images of the cross-sectional distribution of ice at the shutdown after the cold start at −20 °C and −10 °C.

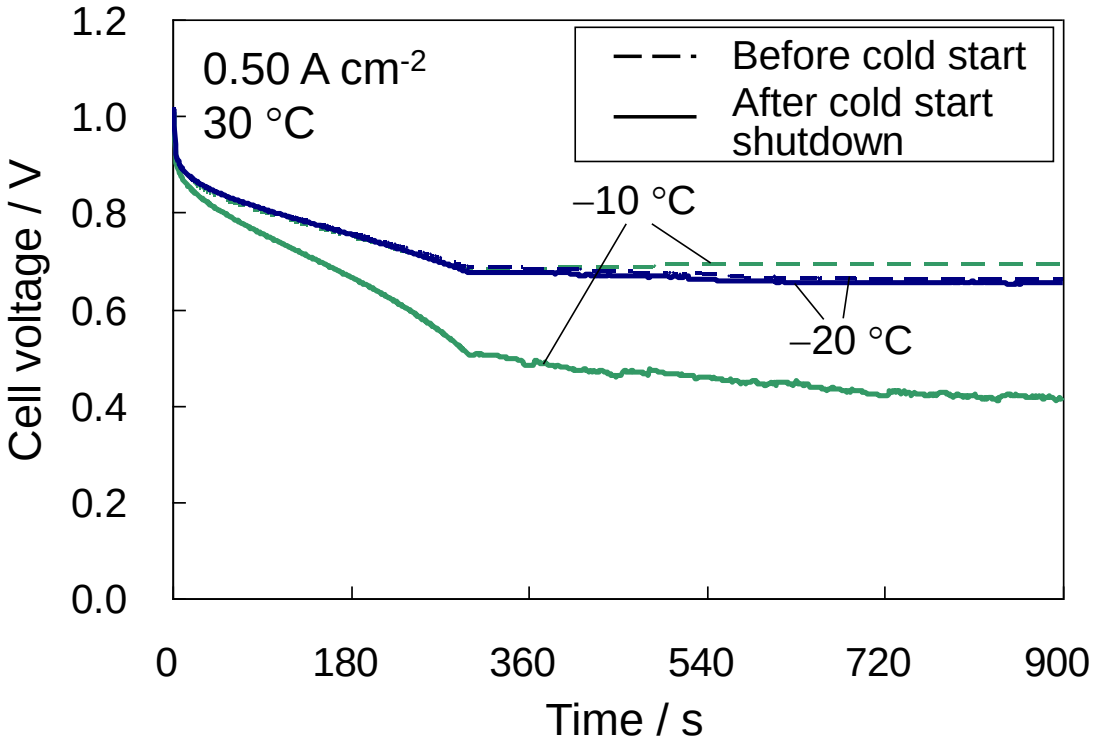

Fig. 10. Plot of the cell performance at 30 °C before and after the occurrence of shutdown due to the cold start at −20 °C and −10 °C.

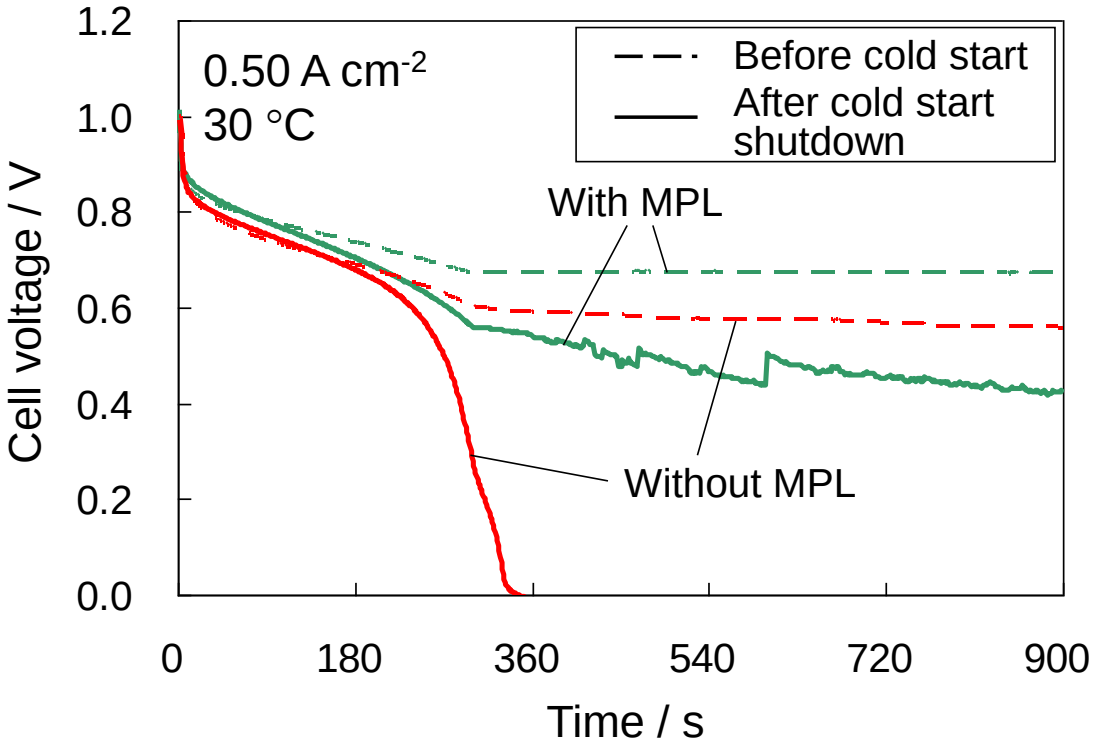

Fig. 11. Plot of the cell performance at 30 °C before and after the occurrence of shutdown due to the cold start with and without the MPL.

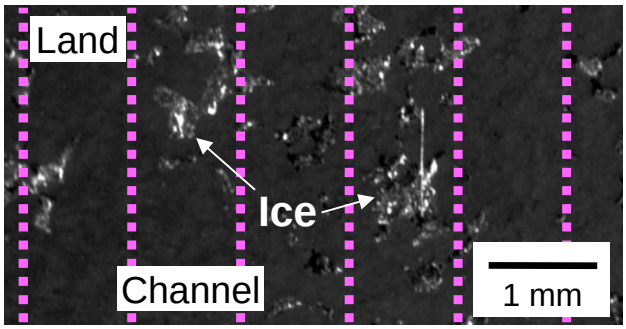

(a) With MPL

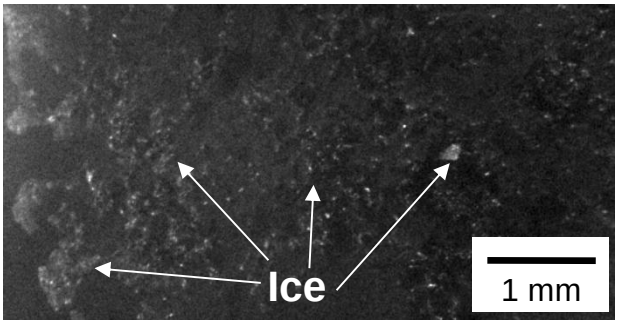

(b) Without MPL

Fig. 12. Photos of the cathode catalyst layer surface after the shutdown of the cold start at −10°C with and without the MPL.

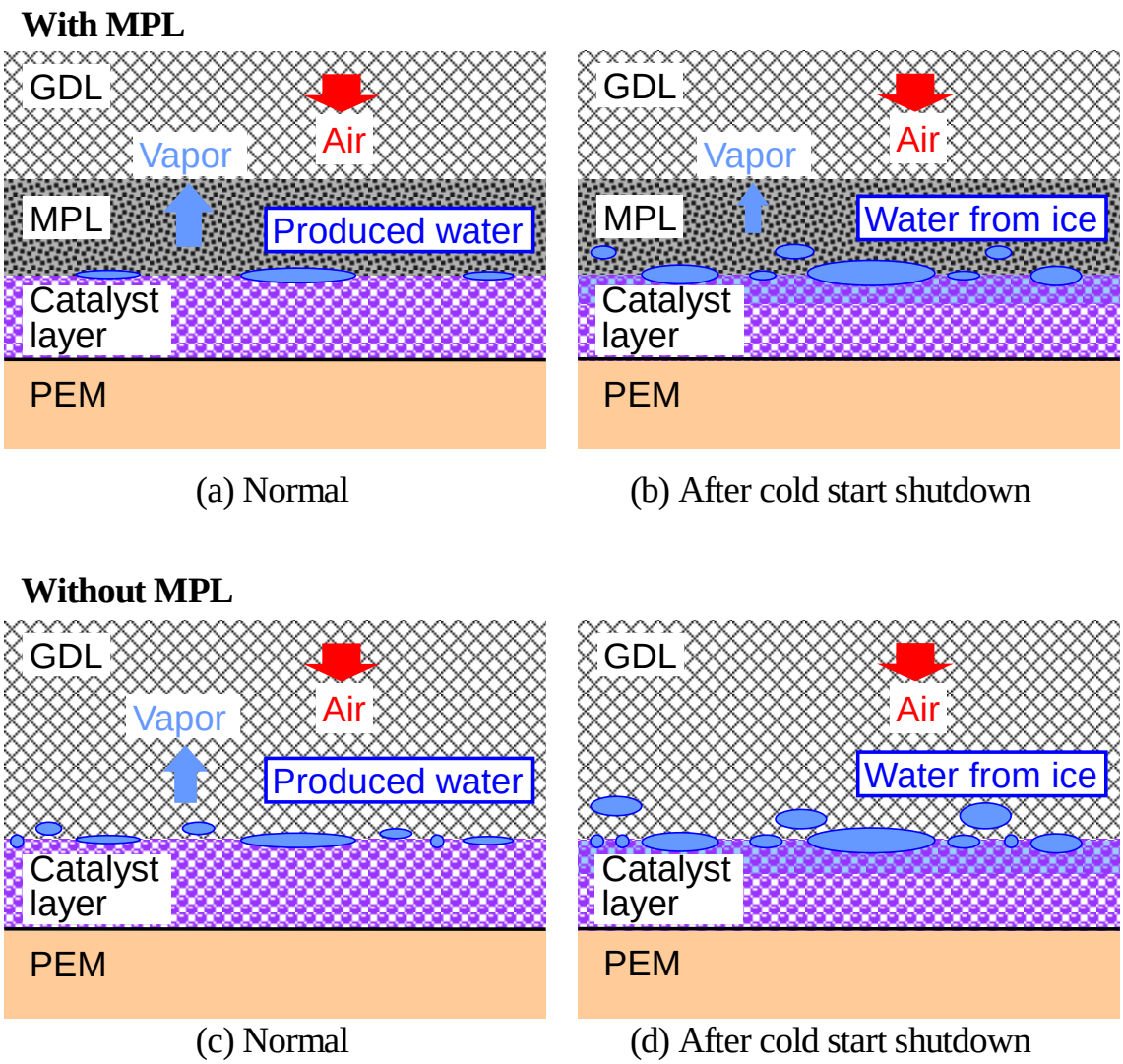

Fig. 13. Experimentally suggested images of the cross-sectional distribution of liquid water at normal operation and after the cold start shutdown operation.

Table 1 Amount of the residual water generated in the total operation and after the membrane rehydration.

Current density [A cm^{-2}]			0.01	0.02	0.04	0.08	0.12
Residual water [mg cm^{-2}]	Total operation	–20 °C	1.51	1.31	1.26	-	-
		–10 °C	-	-	2.28	2.41	2.52
	After membrane rehydration	–20 °C	0.680	0.435	0.298	-	-
		–10 °C	-	-	0.721	0.537	0.439